International Journal of Heat and Technology
Vol. 44, No. 3, June, 2026, pp. 1043-1054
Journal homepage: http://iieta.org/journals/ijht

Numerical Investigation of Refractory Degradation in Industrial Furnaces via Coupled Turbulent Reacting Flow and Heat Transfer Modelling

Manoj Kumar Panda[1], Pruthiviraj Nemalipuri[1*], Vasujeet Singh[1], Vivek Vitankar[2], Harish Chandra Das[1], Malay Kumar Pradhan[3]

[1] Department of Mechanical Engineering, National Institute of Technology Meghalaya, Shillong 793003, India
[2] FluiDimensions, Pune 411045, India
[3] Directorate of Factories & Boilers, Govt of Odisha, Bhubaneswar 751001, India

Corresponding Author Email: pruthivirajnemalipuri@gmail.com

https://doi.org/10.18280/ijht.440313

Received: 13 April 2026
Revised: 8 June 2026
Accepted: 21 June 2026
Available online: 30 June 2026

Keywords:
Computational Fluid Dynamics, Eulerian-Lagrangian, evaporation, combustion, fired furnace, refractory failure

ABSTRACT

Refractory brick failure in fired furnaces significantly degrades thermal efficiency, increases maintenance costs, and leads to unplanned operational downtime in process industries. This study presents an industrially validated Computational Fluid Dynamics (CFD) methodology to diagnose and mitigate refractory degradation caused by localized heat accumulation and hotspot formation. A detailed CFD simulation is performed on Sulphuric Acid Regenerator (SAR) at Indian Oil Corporation Limited (IOCL), Paradeep, using Siemens Simcenter STAR-CCM+. Liquid spent injection, gas-phase combustion and hotspot prediction are modelled using an Eulerian–Lagrangian multiphase framework coupled with the Eddy Break-Up combustion approach, enabling a realistic representation of industrial firing conditions. The novelty of this work lies in the coupled evaluation of thermal and aerodynamic loads on refractory linings, accounting simultaneously for flue gas temperature fields, flow velocity, and gas trajectory effects responsible for accelerated refractory wear. The simulations accurately identify critical hotspot regions. Based on CFD-derived insights, targeted design modifications, including optimized refractory replacement in the SAR, are proposed and implemented. The results demonstrate measurable improvement in refractory reliability and operational lifespan, establishing CFD as a powerful, predictive tool for failure prevention and design optimization in high-temperature industrial furnaces, with immediate applicability to refinery and petrochemical operations.

1. INTRODUCTION

Refractory materials are essential in fired furnaces because of their ability to withstand extreme temperatures and chemically aggressive environments, often exceeding 1400 °C [1-3]. They serve as protective barriers, safeguarding furnace shells and downstream equipment from high-temperature flue gases, molten phases, and entrained particulates. Despite their inherent thermal stability and chemical resistance, refractory linings are susceptible to degradation when exposed to prolonged thermal and mechanical stresses. Premature failure caused by excessive heat accumulation and localized hotspot formation remains a major operational concern across industries such as oil and gas, fertilisers, coal-fired power generation, cement, waste incineration, and metallurgy [4]. In industrial furnaces, refractory linings are subjected to complex erosion processes driven by coupled chemical and mechanical effects. Chemical attack from molten slag, reactive gases, and salts, along with mechanical damage due to high-velocity particle impingement, slag flow, creep, thermal shock, and spalling, accelerates material deterioration [5-8]. Among these, high-temperature erosion is particularly severe, as it weakens the refractory structure and significantly reduces its service life [4, 9, 10]. Field observations indicate that refractory failures often occur at temperatures above 1100 °C, primarily due to sustained heat accumulation and the presence of high-melting impurities and limestone particles introduced during desulphurization [11-14]. Similar degradation patterns are observed in cement kilns, cyclone separators, and waste incinerators, where exposure to clinker, ash, dust, and heterogeneous feed streams imposes intense thermal and mechanical loads [1, 5, 14-17]. Such failures result in unplanned shutdowns, increased maintenance requirements, reduced plant availability, and substantial economic losses [9, 18-23]. Although the interaction between flue gases and refractory linings plays a critical role in wear progression, furnace design and troubleshooting still rely heavily on empirical approaches and post-failure analyses [4, 24-27]. As a result, predictive understanding of flow distribution, heat transfer, and localized thermal loading remains limited. Most existing studies have concentrated on particle impact erosion, with relatively few addressing degradation caused by heat accumulation and hotspot formation. Furthermore, previous investigations on fired furnaces have largely focused on

combustion efficiency and fuel chemistry [13, 20, 22, 24], often neglecting the direct coupling between combustion-induced flow structures, heat transfer, and refractory thermal stresses [3, 4, 6]. This gap is significant, as localized hotspots rather than average furnace temperatures are typically responsible for refractory cracking, spalling, and premature failure.

The present study addresses this gap by developing a standardized, industry-scale computational framework that directly links liquid fuel combustion dynamics with refractory heat buildup and hotspot formation. Unlike conventional Computational Fluid Dynamics (CFD) studies centred on combustion alone, this work treats refractory integrity as a key performance parameter. The methodology integrates an Eulerian–Lagrangian multiphase approach to capture fuel atomization and evaporation, along with turbulence chemistry interaction modelling using the Eddy-Breakup model and the Realizable k–ε turbulence model, as shown in Figure 1. This combined approach enables high-fidelity prediction of flow behaviour and localized thermal loads on refractory surfaces. A notable contribution of this work is the validation of grid-independent CFD results against real-time operating data from Indian Oil Corporation Limited (IOCL), Paradeep, India an aspect rarely reported in refractory-focused studies. This validation enhances the credibility and industrial applicability of the methodology. The validated simulations are then used to identify critical hotspot regions responsible for refractory damage.

Figure 1. Computational Fluid Dynamics (CFD) methodology for the analysis of a fired furnace

Importantly, the insights obtained from CFD analysis are translated into practical design modifications implemented in the operating Sulphuric Acid Regenerator (SAR) unit. These modifications demonstrate the effectiveness of CFD as a proactive tool for mitigating heat accumulation, reducing thermal stresses, extending refractory life, and improving furnace reliability. Overall, the proposed methodology provides a scalable and transferable framework for addressing refractory degradation across a wide range of high-temperature industrial systems, delivering improvements in operational safety, energy efficiency, and lifecycle cost reduction.

The paper starts with a general overview of fired furnaces, focusing on how important they are to processes and the main reasons why refractory lining breaks down in very hot and acidic conditions. In Section 2, we discuss extensive detail about the numerical framework. This includes the discretisation strategy, the pressure–velocity and phase-coupling methodologies, and the multiphase reacting flow formulation based on a Eulerian–Lagrangian approach. The governing conservation equations for mass, momentum, energy, and species transport are systematically described to show the rigorous CFD modelling. A thorough CFD study of the SAR is then performed, and it is carefully checked against industry-scale operating data from IOCL, Paradeep, to make sure it is both physically accurate and useful in the real world. Section 3 deals about the modification in the regenerator and its affects on the hotspot formation, combustion behaviour, and thermal loading.

2. NUMERICAL MODELLING AND SIMULATION

This study applies CFD to take a closer, physics-based look at how heat and flow behave inside an H_2SO_4 regenerator, using Simcenter STAR-CCM+. CFD is chosen here not just as a numerical tool, but as a way to capture the real complexity of furnace operation, where turbulent combustion chemistry and heat transfer interact simultaneously and ultimately control the furnace operation. Also, the CFD allows modelling the physics inside the refractory as a separate physics during the simulation. The models for the refractory bricks consider the solid-state physics with all its properties. It participates in the heat transfer from the furnace internals through the refractory. By utilising the two physics models, Fluid and Solid, we can model how and where the refractory lining fails.

To replicate the furnace geometry as of the plant, a detailed three-dimensional model of the regenerator is prepared using the dimensions of General Arrangement drawings provided by IOCL, Paradeep as shown in Figure 2. This level of geometric fidelity matters more than it might seem at first glance. In large industrial furnaces, even small asymmetries, slight shifts in burner position, or minor geometric irregularities can distort the flow field enough to create uneven heat distribution. The model, therefore, captures these details so that the simulation reflects what actually happens inside the operating unit, not an idealized version of it. The simulations focus on predicting temperature and velocity tracks inside the furnace, since these directly determine how heat is transferred to the refractory walls. What emerges is a clear picture of how certain flow dynamics and temperature attainment drive localized heat buildup. These regions intensify convective heat transfer toward the walls. The result is the formation of hotspots, which are the primary precursors to refractory damage. By mapping liquid particle velocity patterns alongside wall temperature distributions, the study connects the “flow physics” to the “failure locations” in a very direct and intuitive way.

With this understanding, the work moves beyond diagnosis to solution. Geometry modifications are proposed within the furnace enclosure to reshape the flow field, essentially spreading thermal energy more evenly. These changes are not arbitrary; they are guided by the physics observed in the simulations. The modified design shows a much more uniform temperature distribution along the refractory lining, indicating a significant reduction in hotspot intensity. In practical terms, this means the refractory is subjected to less thermal stress concentration, which should translate to longer service life, fewer unexpected shutdowns, and more stable long-term operation. The study therefore demonstrates how CFD can move from being a diagnostic tool to a decision-making tool, bridging the gap between flow physics and real industrial reliability.

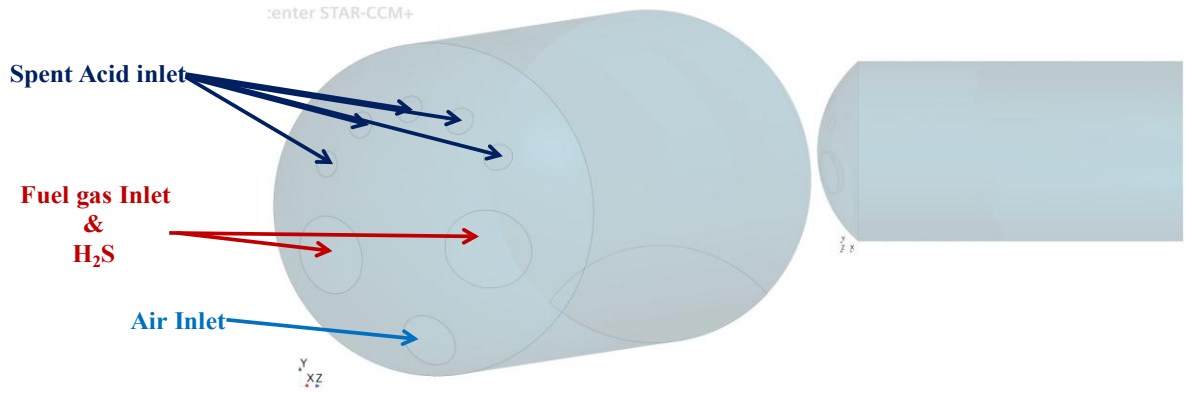

Figure 2. 3D CAD with spent acid, air, and fuel inlet ports arrangements of H_2SO_4 regenerator

2.1 Discretisation

In CFD, discretization is fundamentally about how well the governing conservation laws: mass, momentum, energy, and species are represented over a finite set of control volumes. The mesh is not just a numerical convenience; it defines how accurately gradients, fluxes, and source terms are resolved in space. If the mesh does not faithfully capture these variations, the solution may satisfy the discretized equations but fail to represent the true physics. From a physical standpoint, flow and thermal fields in furnaces are dominated by steep spatial velocity gradients, temperature gradients near flame fronts, and heat transfer near refractory walls. Accurately resolving these requires a mesh that can capture both the magnitude and direction of gradients. For example, excessive cell skewness distorts the alignment between the true gradient vector and its numerical approximation, directly affecting diffusive and convective flux calculations. Similarly, abrupt changes in cell size can introduce artificial numerical diffusion or dispersion, smearing sharp features such as flame zones or mixing layers. Grid density, therefore, must be guided by physics rather than uniform refinement. Regions with high strain rates, intense mixing, or strong heat release, such as burner jets and recirculation zones, demand finer resolution to correctly predict turbulence-chemistry interaction and scalar dissipation rates. Near-wall regions require adequate resolution to capture boundary layer development and wall heat flux, especially when conjugate heat transfer and radiation are important. In combustion-dominated systems, the coupling between flow, reaction kinetics, and heat transfer makes the solution particularly sensitive to discretisation quality. An under-resolved mesh may misrepresent flame stabilization mechanisms, alter reaction rates through incorrect temperature fields, and consequently distort radiative heat transfer to the refractory. These errors are not merely numerical; they propagate through the coupled physics and lead to incorrect predictions of hotspot formation and thermal loading. Thus, mesh quality directly governs how well the discrete system preserves the underlying physical balances. A physically informed meshing strategy ensures that key transport processes and interactions are resolved with sufficient fidelity, enabling the simulation to reproduce not just convergence, but the correct physics driving the system.

Polyhedral meshes have become increasingly preferred in CFD not just for convenience, but because they align well with how transport processes actually behave in complex flows. In a finite-volume method, the accuracy of any solution depends on how well gradients and fluxes are reconstructed across control volumes. Polyhedral cells naturally improve this reconstruction because each cell shares faces with a larger number of neighbouring cells compared to tetrahedral or hexahedral elements. This richer connectivity provides more directional information, allowing gradients of velocity, temperature, and species to be estimated more accurately. From a physical perspective, this matters most in regions where the flow is highly three-dimensional and strongly coupled, such as in reacting flows, recirculation zones, and flame regions inside furnaces. Here, transport is not aligned along simple coordinate directions; it is multidirectional, with convection, diffusion, and reaction all interacting. Polyhedral cells, by virtue of their geometry, are better suited to capture these multidirectional gradients without introducing excessive numerical diffusion.

As a result, sharp features like flame fronts, shear layers, and thermal gradients are preserved more faithfully. Another important advantage is efficiency. Because each polyhedral cell carries more topological information, fewer cells are typically needed to achieve the same level of accuracy. This reduces the overall cell count without compromising physical resolution, leading to lower computational cost. At the same time, the improved connectivity between cells enhances the stability of the numerical solution. Information propagates more smoothly across the domain, which helps the solver converge faster and reduces sensitivity to mesh-induced errors. Polyhedral meshes also adapt well to the irregular geometries commonly found in industrial furnaces, burner assemblies, curved enclosures, and refractory linings. Instead of forcing excessive local refinement to fit these shapes, polyhedral cells conform more naturally, maintaining mesh quality even in geometrically complex regions. This is particularly important when near-wall heat transfer and radiative exchange are critical, as poor geometric representation can directly affect predicted wall heat flux. In essence, polyhedral meshing offers a physically meaningful advantage: it improves how gradients and fluxes are represented while keeping the computational effort manageable. This makes it especially effective for large-scale, turbulence-driven, multiphase combustion problems, where both accuracy and efficiency are equally important.

2.2 Setup and solution

In this study, the combustion behaviour of the SAR is analysed using actual operating conditions obtained from IOCL, Paradeep. This ensures that the simulations closely represent real plant conditions rather than idealized assumptions. The boundary conditions applied in the model are detailed in Table 1. All simulations were carried out on a

high-performance computing system equipped with an Intel i7 (12th generation) processor, 24 cores, and 64 GB of RAM, providing the necessary computational capability to resolve the complex, coupled thermo-fluid processes involved in the furnace.

Table 1. Boundary conditions

Boundary Conditions	Value	Temperature
Spent acid flow rate	2.268612 kg/sec	311 K
Fuel gas flow rate	0.129392 kg/sec	313 K
Air flow rate	4.42225 kg/sec	922 K

2.3 Mathematical modelling

Complex industrial processes involving fluid flow, heat transfer, and combustion are fundamentally governed by nonlinear partial differential equations. These equations represent the conservation of mass, momentum, energy, and chemical species within the system. However, due to the strong coupling between flow turbulence, chemical reactions, heat release, and multiphase interactions, obtaining analytical solutions for such practical engineering problems is nearly impossible. CFD provides a powerful numerical framework to overcome this limitation by discretizing the governing differential equations into a finite set of algebraic equations using numerical techniques such as the finite volume method. These discretised equations are then solved iteratively to obtain the flow, temperature, and species fields throughout the computational domain.

In the present study, combustion of fuel gas with air is modelled using the Eddy-Breakup model inside the fired furnace. The heat produced in the combustion of fuel gas will be utilised for the decomposition of H_2SO_4. The Eulerian-Lagrangian multiphase approach is utilised to capture the decomposition of H_2SO_4 to H_2O and SO_2. Physically, the spent acid enters the furnace in the form of droplets, while the surrounding air exists as a continuous fluid medium.

Since the behaviour of these two phases differs significantly in terms of momentum, heat transfer, and transport characteristics, an Eulerian–Lagrangian framework is employed for accurate representation of spent acid injection and decomposition. Within this approach, the gaseous phase is treated as a continuous medium using the Eulerian formulation, where the governing equations are solved throughout the computational domain. In contrast, the liquid spent acid droplets are treated as discrete particles and tracked individually using a Lagrangian framework. The motion of each droplet is governed by the particle force balance, which accounts for aerodynamic drag, inertia, gravity, and other relevant forces acting on the particles.

The dynamics of the dispersed liquid phase and the continuous gas phase are strongly coupled and therefore must be solved simultaneously. From a physical standpoint, the surrounding airflow determines the trajectories, residence time, mixing behaviour, evaporation rate, and dispersion of the acid droplets. Simultaneously, evaporation of the droplet releases mass, momentum, and energy into the gas phase, thereby altering the local flow and temperature fields. This two-way interaction between the phases makes a coupled solution of the governing equations essential for accurately predicting flame structure, heat transfer, combustion stability, and pollutant formation inside the furnace.

Gas-phase governing equations:

The continuous gas phase is solved using the fundamental conservation equations of fluid dynamics. The conservation of mass equation ensures that mass is neither created nor destroyed within the computational domain. The conservation of momentum equation, derived from the Navier–Stokes equations, governs the transport of momentum under the influence of pressure gradients, viscous stresses, turbulence, and external body forces. Since combustion is an exothermic chemical phenomenon involving substantial heat release, the conservation of energy equation is solved to predict the temperature distribution and heat transfer characteristics within the furnace. Physically, this equation accounts for convective and conductive heat transport, heat generated due to chemical reactions, and radiative heat exchange occurring at high-temperature combustion conditions. During combustion, multiple chemical species are continuously formed and consumed through oxidation and intermediate reaction pathways. Therefore, species transport equations are solved to model the transport, diffusion, mixing, and chemical conversion of individual species within the flow field. These equations are essential for accurately capturing combustion efficiency, flame behaviour, pollutant formation, and overall furnace performance.

Mass conservation:

$$\frac{\partial \rho}{\partial t} + \nabla \cdot (\rho \vec{v}) = S_m \tag{1}$$

Momentum conservation:

$$\frac{\partial}{\partial t}(\rho \vec{v}) + \nabla \cdot (\overrightarrow{\rho v v}) = -\nabla p + \nabla(\vec{\tau}) + \rho \vec{g} + \vec{F} \tag{2}$$

Energy conservation:

$$\frac{\partial}{\partial t}(\rho E) + \nabla \cdot \left(\vec{v}(\rho E + p)\right) = \nabla \cdot (k_{eff} \nabla T - \Sigma_j h_j \vec{J_J} + (\tau_{eff} . \vec{v}) + S_h) \tag{3}$$

Species conservation:

$$\frac{\partial}{\partial t}(\rho Y_i) + \nabla \cdot (\rho \vec{v} Y_i) = -\nabla \cdot J_i + R_i + S_i \tag{4}$$

Turbulent kinetic energy (k):

$$\frac{\partial}{\partial t}(\rho k) + \nabla \cdot (\rho k \vec{v}) = \nabla \cdot \left[\left(\mu + \frac{\mu_t}{\sigma_k}\right) \nabla k\right] + P_k - \rho(\varepsilon - \varepsilon_0) + S_k \tag{5}$$

Turbulent kinetic dissipation rate (ε):

$$\frac{\partial}{\partial t}(\rho \varepsilon) + \nabla \cdot (\rho \varepsilon \vec{v}) = \nabla \cdot \left[\left(\mu + \frac{\mu_t}{\sigma_\varepsilon}\right) \nabla \varepsilon\right] + \frac{1}{T_e} C_{\varepsilon_1} P_\varepsilon - C_{\varepsilon_2} f_2 \rho \left(\frac{\varepsilon}{T_e} - \frac{\varepsilon_0}{T_0}\right) + S_\varepsilon \tag{6}$$

Combustion modelling:

For the fuel gas combustion in the furnace, the Eddy Break-Up combustion model is utilized. The chemical reaction of the fuel is turbulence-driven combustion. This model is most useful for non-premixed combustion.

The time-averaged of the instantaneous governing equations is given by:

$$\frac{\partial}{\partial t}(\rho \chi Y_i) + \nabla \cdot (\rho U \bar{Y}_i - \bar{F}_i) = \bar{s}_i \tag{7}$$

where, F_i is diffusion flux modeled as:

$$F_i = \left(D_i + \frac{\mu_t}{s_{c_i}}\right)\nabla\overline{Y_i} \tag{8}$$

The rate of fuel consumption is given by:

$$R_F = R_{F,mix} = -\frac{\rho}{M_F}\left(\frac{1}{\tau_R}\right)A_{ebu}\, min\left\{\overline{Y}_F, \frac{\overline{Y_o}}{s_o}\right\} \tag{9}$$

Quasi-steady evaporation:

The quasi-steady evaporation model is widely used to describe mass transfer from liquid droplets to the surrounding gas phase during spray in the fired furnace. In this model, liquid particles continuously lose mass through evaporation as they interact with the hot gaseous environment. Physically, evaporation occurs because the liquid–vapour system surrounding the droplet is not in thermodynamic equilibrium. When a liquid droplet is exposed to a high-temperature gas environment, the vapour concentration at the droplet surface becomes higher than that in the surrounding gas phase, creating a concentration gradient that drives mass transfer from the droplet surface into the gas phase. The evaporation process is governed by the coupled effects of heat transfer and mass diffusion. Heat from the surrounding hot gases is transferred to the droplet surface, providing the latent heat required for phase change, while vapour molecules diffuse away from the droplet into the surrounding gas. Thus, droplet evaporation is fundamentally controlled by the balance between thermal energy supplied to the droplet and the rate at which vapour is transported away from the interface. The liquid–vapour equilibrium is generally represented using an idealized phase diagram, where the evaporation characteristics are primarily determined by two important thermophysical properties of the liquid fuel: the saturation pressure and the critical temperature. The saturation pressure defines the tendency of the liquid to vaporize at a given temperature, whereas the critical temperature represents the thermodynamic limit beyond which distinct liquid and vapour phases no longer exist. These properties are incorporated into the material definition of the Lagrangian phase to accurately model evaporation behaviour under furnace operating conditions. In the quasi-steady evaporation formulation, the evaporation process is assumed to occur under quasi-equilibrium conditions around the droplet surface. The model further assumes that the droplet is internally homogeneous and composed of a single liquid component, such as an individual chemical species. This implies that temperature and composition gradients inside the droplet are neglected, allowing the droplet properties to remain spatially uniform at any instant of time. Such an assumption is physically reasonable for sufficiently small droplets where internal mixing and thermal diffusion occur much faster than the external evaporation timescale. Under these assumptions, the rate of droplet mass reduction due to evaporation is governed by the balance between vapour diffusion from the droplet surface and convective transport into the surrounding gas phase. Consequently, the rate of change of droplet mass due to quasi-steady evaporation ($\dot{m_p}$) can be expressed as:

$$m_p = -g^* A_s ln(1+B) \tag{10}$$

where, B is the Spalding transfer number and g* is the mass transfer conductance (to be precise, in the limit B→0).

The conductance will be:

$$g^* = \frac{kNu_p}{c_p D_p} \tag{11}$$

The transfer number will be:

$$B = \frac{Y_{v,s} - Y_v}{1 - Y_{v,s}} \tag{12}$$

where, Y_v is the vapour mass fraction in the $Y_{v,s}$ is the surface equilibrium vapour mass fraction.

$$\mathrm{Y_{v,s}} = \mathrm{X_{v,s}}\frac{\mathrm{W_v}}{\mathrm{W_s}} \tag{13}$$

where, W_v and W_s are the molecular weights of the vapour and gas mixture at the droplet surface, respectively.

Finally, the conductance will be:

$$g^* = \frac{\rho D_v Sh_p}{D_p} \tag{14}$$

Besides the driving force, two other important parameters in determining the droplet evaporation rate are the molecular diffusivity of the gas component and the Sherwood Number of the droplet.

The Sherwood number can be calculated using the Ranz Marshall correlation:

$$Sh_p = 2\left(1 + 0.3Re_p^{1/2}Sc^{1/3}\right) \tag{15}$$

Radiation model:

Radiation is of great importance in high-temperature process, where the gas molecules and particles are highly energized and generate substantial amounts of radiation. The chemical processes of flame are greatly aided by radiation. Dissociation or ionization of molecules or atoms by radiation, for instance, can result in the creation of radicals or other reactive species. Because of this, the combustion chemistry may be affected. The participating media effects is modelled using the Discrete Ordinate Method (DOM). The radiative flux divergence is a crucial term in the gas-phase energy equation, which describes the relationship between combustion, thermal radiation and the energy in the gas phase. The material in between absorbs radiation as it passes through a medium, increasing its radiant intensity I in that direction. The radiative transfer equation (RTE) drives this process. At a particular wavelength, the following equation can be expressed in terms of radiant intensity:

$$\frac{dI_\lambda}{ds} = -B_\lambda I_\lambda + k_{a\lambda}I_{b\lambda} + \frac{k_{s\lambda}}{4\pi}\int_0^{4\pi} I_\lambda \Omega\, d\Omega + k_{pa\lambda}I_{pb\lambda} + \frac{k_{ps\lambda}}{4\pi}\int_0^{4\pi} I_\lambda \Omega\, d\Omega \tag{16}$$

The radiative transport equation (RTE) system is solved using the DOM approach. The RTE being solved in DOM model includes a finite number of discrete solid angles, each with a vector direction s fixed in the global Cartesian system (x, y, z). The DOM model considers the radiative transfer equation (RTE) for each wavelength band:

$$s_i.\nabla I_{i\Delta\lambda} = -\beta_{\Delta\lambda} I_{i\Delta\lambda} + k_{a\Delta\lambda} I_{b\Delta\lambda} + \frac{k_{s\Delta\lambda}}{4\pi}\sum_{j=1}^{n} w_j I_{j\Delta\lambda} + \bar{k}_{p\Delta\lambda} I_{p\Delta\lambda} + \frac{\bar{k}_{p\Delta\lambda}}{4\pi}\sum_{j=1}^{n} w_j I_{j\Delta\lambda} \quad (17)$$

Here, $\Delta\lambda$ represents the wavelength band from λ_m to λ_n.

3. RESULTS AND DISCUSSIONS

3.1 Computational Fluid Dynamics analysis of Sulphuric Acid Regenerator

The H_2SO_4 regenerator plant is designed to recover sulphur from both spent acid streams and hydrogen sulfide (H_2S)-rich off-gases generated within the refinery. The recovered sulphur is converted back into sulphuric acid and recycled to the refinery, thereby improving sulphur recovery efficiency while minimizing waste generation. In addition to recovering sulphur from spent alkylation acid, the process also utilizes SO_2-rich gas streams to compensate for sulphur demand beyond the available spent acid capacity of 196 MTPD (90% basis) or 176.4 MTPD (100% basis). At the core, the process is a decomposition furnace, where spent sulphuric acid is atomized through spray nozzles into a high-temperature reacting environment. Under these conditions, the acid undergoes thermal decomposition to form sulphur dioxide (SO_2), oxygen, and water vapour. The decomposition process is highly endothermic and therefore requires a continuous supply of thermal energy. Part of this energy demand is naturally fulfilled by the combustion of hydrocarbons present in the spent acid stream, producing carbon dioxide and water vapour while simultaneously contributing to furnace heating. Additional thermal energy is supplied through the combustion of H_2S gas injected into the furnace through dedicated burner nozzles. The oxidation of H_2S generates SO_2 and water vapour while releasing substantial heat, thereby supporting the thermal decomposition reactions. Any hydrocarbons present in the H_2S stream behave similarly to those in the spent acid feed, contributing additional combustion energy to the system. To maintain stable process conditions, supplementary fuel gas combustion is employed whenever the heat generated from acid decomposition and H_2S oxidation becomes insufficient. This ensures that the furnace outlet temperature remains close to 1066 ℃, which is critical for complete decomposition and stable downstream operation. From a thermochemical standpoint, maintaining this temperature is essential because lower temperatures can reduce reaction completeness and promote undesirable sulphur condensation in downstream equipment.

The combustion air supplied to the furnace is preheated to approximately 649 ℃ using a fuel-fired air preheater before entering the decomposition furnace. Preheating the combustion air significantly improves thermal efficiency by reducing the additional fuel required to sustain the target furnace temperature. Physically, higher inlet air temperature increases the enthalpy of the reactant mixture, thereby reducing the net external energy demand while also lowering the overall gas volume handled by downstream equipment. The process air fan delivers the required oxygen for combustion through the preheater and into the furnace. Careful oxygen control is crucial for maintaining stable furnace chemistry and process reliability. The decomposition furnace exit gas is typically maintained at approximately 2.5% excess oxygen on a dry basis. If oxygen levels become too low, incomplete oxidation may occur, leading to the formation of elemental sulphur. Since sulphur can condense at lower temperatures, this may result in deposition and plugging in downstream heat recovery equipment. Conversely, excessive oxygen dilutes the SO_2 concentration, increases volumetric gas flow through the plant, and enhances SO_3 formation, ultimately increasing acid losses and reducing overall process efficiency. The furnace operation is regulated through a relatively simple but effective control strategy. Overall plant throughput is controlled through the main gas blower flow rate, while the H_2S feed rate is maintained at a level sufficient to compensate for sulphur losses in the process. Fuel gas flow is automatically adjusted to maintain the desired excess oxygen concentration at the furnace outlet, whereas the spent acid feed rate is controlled to sustain the target outlet temperature of 1066 ℃. The high-temperature decomposition gases exiting the furnace subsequently pass through a fire-tube waste heat boiler and a superheater, where thermal energy is recovered from the flue gases. However, the extent of cooling is carefully limited by the acid dew point and the metallurgical constraints of the heat exchanger materials. Excessive cooling can lead to acid condensation and severe corrosion, making thermal management in these sections particularly critical for long-term plant reliability and operational safety.

A detailed CFD investigation was carried out to understand and resolve the thermal issues observed in the SAR furnace. The study systematically examined the influence of combustion air flow, spent acid injection, and fuel gas supply under different geometric configurations of the furnace. The objective was not only to identify the source of refractory overheating, but also to understand the underlying flow and heat transfer mechanisms responsible for hotspot formation. To accurately represent the multiphase nature of the process, an Eulerian–Lagrangian framework was adopted. In this approach, the continuous gaseous phase is solved in the Eulerian reference frame, while the injected sulphuric acid droplets are individually tracked in a Lagrangian manner. Physically, this is important because the atomized acid droplets experience complex interactions with the surrounding high-temperature combustion gases, including momentum exchange, heating, evaporation, and mixing. The evaporation of sulphuric acid droplets was modelled using a quasi-steady evaporation approach. This model assumes that, although the surrounding gas-phase flow field may vary rapidly due to turbulence and combustion, the evaporation process occurring at the droplet surface reaches a local steady state over relatively small timescales. Such an assumption is well suited for high-temperature furnace environments, where droplet heating and phase change are primarily governed by convective and thermal diffusion processes. The model, therefore, captures the coupled heat and mass transfer between the liquid droplets and the surrounding gases with reasonable physical accuracy. A two-way coupling strategy was incorporated to account for the interaction between the dispersed liquid phase and the continuous gas phase. This means that the gas flow influences droplet motion, heating, and evaporation, while the evaporating droplets simultaneously modify the surrounding flow field through momentum, mass, and energy exchange. From a physical perspective, this coupling is essential because droplet evaporation locally alters gas temperature, density, and species concentration, which in turn affects turbulence intensity, combustion behaviour, and heat transfer inside the furnace. The combustion process of the fuel gas was simulated using

the Eddy-Breakup combustion model, which is particularly suitable for turbulence-controlled combustion systems. In industrial furnaces operating under highly turbulent conditions, the overall combustion rate is often governed more by turbulent mixing than by finite-rate chemical kinetics. The Eddy-Breakup model therefore, provides an efficient and physically meaningful way to capture the interaction between turbulence and combustion heat release.

The CFD analysis was initially performed on the original furnace geometry to identify the regions responsible for excessive thermal loading. The simulations revealed the formation of localized hotspots, particularly along the curved refractory surfaces, where high-temperature recirculation zones intensified the heat transfer. By correlating velocity fields with wall temperature distributions, the study established a direct link between the internal flow structures and refractory overheating. Based on these insights, several geometric modifications were introduced to alter the flow distribution and reduce localized thermal accumulation. The redesigned configurations effectively redistributed the combustion gases, weakened high-intensity recirculation zones, and promoted a more uniform temperature field inside the furnace enclosure. The simulations provided detailed information on temperature distribution, velocity profiles, and species concentration fields, all of which were critical for understanding the thermo-fluid behaviour of the system. The CFD-driven analysis enabled the transformation of complex flow physics into practical engineering solutions. The proposed design modifications significantly reduced hotspot intensity, improved thermal uniformity across the refractory lining, and are expected to enhance furnace reliability, reduce refractory degradation, and minimise unplanned shutdowns during long-term industrial operation.

3.1.1 Grid-independence study

A grid independence study is an essential step in CFD analysis because it establishes whether the numerical solution truly represents the underlying physics or is still influenced by mesh resolution. In reacting flow simulations, especially those involving combustion and strong thermal gradients, the predicted flow and temperature fields can become highly sensitive to discretisation. Therefore, demonstrating mesh independence is critical to ensure that the obtained results are physically reliable and not merely numerical artefacts. In the present study, four progressively refined mesh configurations consisting of approximately 0.9856 million, 1.4785 million, 2.2177 million, and 3.3266 million cells were evaluated to assess the sensitivity of the solution to mesh density. The variation of key thermo-fluid parameters with respect to mesh refinement is summarized in Table 2. From a physical perspective, mesh refinement improves the solver's ability to resolve steep velocity and temperature gradients, particularly in regions dominated by turbulent mixing, flame interaction, recirculation, and wall heat transfer. Coarser meshes tend to introduce excessive numerical diffusion, which can artificially smooth temperature peaks, weaken recirculation intensity, and distort heat flux predictions near the refractory walls.

As the mesh becomes finer, these gradients are captured more accurately, leading to more physically consistent predictions of hotspot formation and thermal loading. The comparison between Mesh-1, Mesh-2, and Mesh-3 revealed noticeable variations in the predicted parameters, indicating that the coarser grids were insufficient to fully resolve the dominant transport phenomena inside the furnace. However, the results obtained using Mesh-3 and Mesh-4 are identical. This behaviour indicates that the numerical solution had reached grid-independent convergence, where further mesh refinement no longer produced any meaningful change in the physical solution. Based on this assessment, Mesh-3 was selected for the detailed simulations. This mesh provided an optimal balance between numerical accuracy (approximately 0.2% deviation) and computational efficiency, capturing the critical thermo-fluid structures within the furnace while avoiding the excessive computational expense associated with further refinement. Such a balance is particularly important in large-scale industrial multiphase and combustion simulations, where accurate prediction of flow recirculation, heat transfer, and refractory thermal loading must be achieved within practical computational limits.

3.1.2 Temperature profile

The temperature profile shown in Figure 3 developed inside a SAR is governed by a complex interaction between acid droplet evaporation, gas-phase combustion, radiative heat transfer, turbulent mixing, and endothermic decomposition reactions. Immediately downstream of the burner, atomised spent sulphuric acid droplets undergo rapid heating due to intense convective and radiative energy transfer from the flame envelope. The initial stage is dominated by moisture evaporation, followed by thermal decomposition of sulphuric acid into SO_3 and H_2O, while at elevated temperatures SO_3 further dissociates into SO_2 and oxygen. Since hydrocarbon contaminants present in the spent acid also participate in combustion, a highly reactive flame zone is established near the burner throat, resulting in a sharp rise in temperature. Consequently, the maximum gas temperature is generally observed within the primary combustion region, where localized flame-core temperatures may exceed 1473 K depending on fuel loading and air-to-acid ratio. The strong exothermicity of hydrocarbon oxidation combined with intense turbulent mixing promotes rapid heat release. Radiation becomes the dominant mode of heat transfer at these elevated temperatures, causing substantial thermal loading on refractory linings and generating pronounced radial temperature gradients between the hot flame core and near-wall regions.

Figure 4 presents a comparative correlation between the CFD-predicted temperature field and the actual refractory damage observed inside the SAR, demonstrating a strong thermo-mechanical coupling between localized high-temperature regions and refractory degradation patterns. The temperature contour obtained from the CFD simulation reveals the formation of highly non-uniform thermal zones within the furnace, where localized hot spots exceedingly nearly 1400–1500K are predominantly concentrated along the peripheral wall regions and near the burner interaction zones. These elevated temperature regions correspond remarkably well with the severe refractory spalling, brick collapse, surface vitrification, and structural cracking observed during internal inspection of the regenerator. The strong agreement between simulation and field observations confirms that the refractory deterioration is primarily governed by localized thermal overstressing rather than uniform bulk heating. Physically, the non-uniform temperature distribution originates from complex interactions between turbulent combustion, burner-induced recirculation, radiative heat transfer, and spent acid droplet evaporation dynamics. As the atomised acid droplets enter the furnace, rapid evaporation and decomposition occur in the

vicinity of the flame envelope, while hydrocarbon contaminants present in the acid contribute additional exothermic heat release. The resulting flame-wall interaction produces intense radiative heat flux toward the refractory surface, especially in regions where the swirling flow impinges on the furnace wall. Since thermal radiation scales strongly with temperature, the localized high-temperature flame structures generate disproportionately large wall heat loads, accelerating refractory wear and thermally induced mechanical failure.

Table 2. Grid-independence study of the sulphur furnace

S. No.	Parameter	Real-Time Data (From IOCL)	Mesh-1 (985673)	Mesh-2 (1478510)	Mesh-3 (2217765)	Mesh-4 (3326648)
1	Maximum temperature attained in the furnace	1473 K	1549 K	1512 K	1476 K	1476 K
2	Maximum Temperature at the Outlet	1339 K	1408 K	1365 K	1343 K	1343 K

Note: IOCL: Indian Oil Corporation Limited.

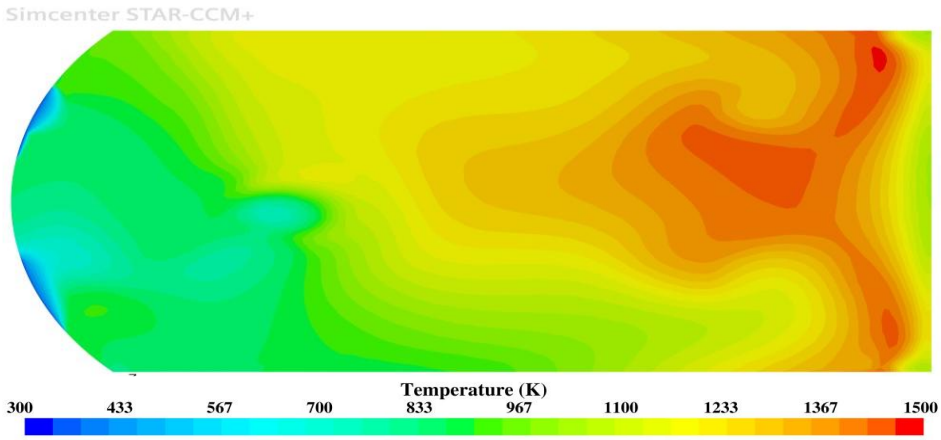

Figure 3. Temperature contour on the central plane of the H_2SO_4 regenerator

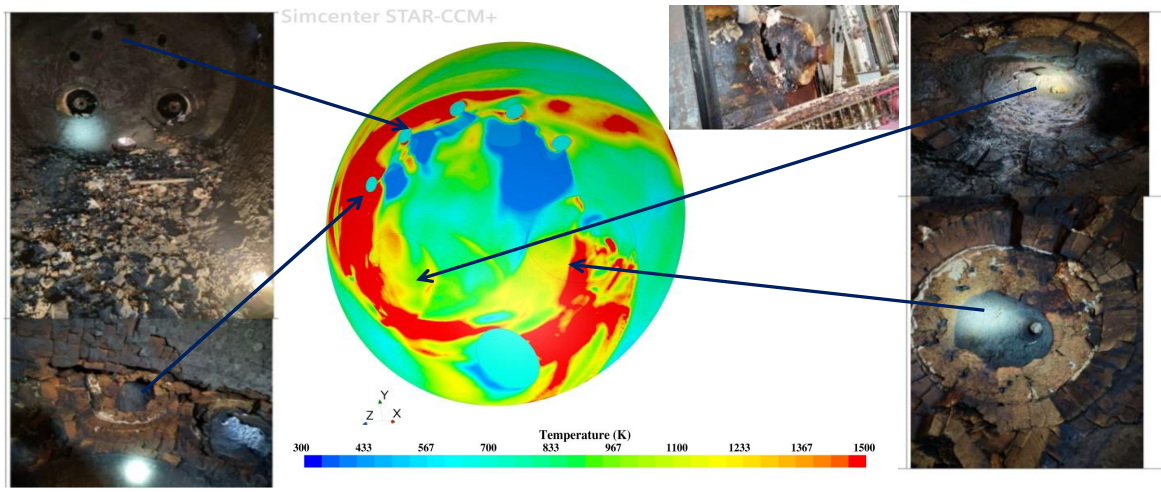

Figure 4. Hotspot formation on the curved surface and corresponding refractory damage

The CFD contour further indicates the presence of asymmetric thermal recirculation zones within the regenerator, which are characteristic of industrial-scale turbulent combustion systems operating under strong swirl conditions. These recirculating structures increase gas residence time and stabilise combustion; however, they also trap high-temperature combustion products near the refractory surface for prolonged durations. Consequently, certain wall regions experience sustained thermal exposure, leading to repeated expansion and contraction cycles during operation and shutdown. Such cyclic thermo-mechanical loading induces tensile stresses within the refractory lining, eventually resulting in crack initiation, brick joint opening, and large-scale spalling, as clearly visible in the inspection photographs. In several locations, the refractory failure appears particularly severe near burner openings and transition zones, suggesting excessive near-wall turbulence intensifying the heat transfer rate beyond the refractory design tolerance. Another important observation from Figure 3 is the existence of comparatively cooler core regions surrounded by high-temperature annular structures near the wall. This behaviour is indicative of strong swirling flow aerodynamics, where centrifugal motion transports hot combustion products outward while relatively cooler gases remain near the central recirculation core. Such a thermal structure is commonly observed in large cylindrical combustion chambers and is particularly detrimental in SAR because the refractory lining becomes directly exposed to the highest thermal intensity. Over prolonged operation, these localized hot bands cause differential thermal expansion within the refractory matrix, weakening the bonding structure

and reducing mechanical integrity. The extensive refractory collapse observed in the images, therefore, represents the cumulative effect of thermal shock, high radiative heat flux, cyclic stress accumulation, and localized overheating.

3.1.3 Modification of the refractory brick material

The replacement of the original silica-rich refractory with a highly alumina-based refractory lining resulted in a substantial alteration in the thermal behaviour of the SAR and played a key role in preventing the formation of localized hotspots in the furnace. Table 3 shows that the old refractory mainly consisted of about 52.6% silica (SiO_2) and 42.2% alumina (Al_2O_3), while the newly installed refractory consists of almost 97.6% alumina with traces of silica and other flux-forming oxides. This change in composition caused a substantial increase in the thermo-mechanical stability of the refractory under the extremely high temperature and corrosive conditions of operation of sulphuric acid regeneration. From the materials physics point of view, silica-rich refractories are generally more susceptible to thermal degradation in high-temperature combustion environments due to the phase transformations of silica and comparatively lower resistance to thermal shock and chemical attack. The volumetric instability of silica-containing refractories during repeated heating and cooling cycles is caused by crystalline phase transitions leading to internal stresses and progressive weakening of the refractory matrix. Moreover, the presence of impurities like iron oxide, titania, and alkali-associated oxides lowers the local softening temperature of the refractory and promotes partial vitrification under intense flame radiation for long durations. This made the old refractory lining very susceptible to localized overheating, crack propagation, surface spalling, and eventual structural collapse in areas exposed to concentrated radiative heat flux.

Table 3. Properties of the old and new refractory material

	Old Refractory	New Refractory
Silica (SiO_2)	52.6%	0.12%
Alumina (Al_2O_3)	42.2%	97.6%
Iron Oxide (Fe_2O_3)	1.4%	0.09%
Titania (TiO_2)	2.3%	0.05%
Lime (CaO)	0.2%	0.04%
Magnesia (MgO)	0.3%	0.16%
Other oxides	0.9%	1.94%

The new high-alumina refractory installed, on the contrary, has much better thermal resistance, structural integrity, and dimensional stability at high temperatures. Alumina has a much higher melting point, less tendency for thermal creep, and higher resistance towards chemical corrosion by sulphur-bearing species than silica-based refractory systems. The silica content is also drastically reduced to minimize the formation of low-melting silicate phases, which are weak points under sustained thermal loading. The new refractory is thus able to sustain the mechanical strength and surface integrity even in the severe conditions of radiative and convective heat transfer in the regenerator.

3.1.4 Temperature profile with modified refractory material

The thermal uniformity and structural stability of the furnace wall were improved after the installation of the high-alumina refractory material. The improved refractory maintained a smoother and more intact hot-face surface, thereby reducing localized flame impingement and minimizing abnormal heat concentration zones. Moreover, the higher thermal stability of alumina enabled the refractory to withstand intense radiative heat flux without undergoing rapid degradation or local softening. The high-alumina refractory material also redistributes the thermal gradient more uniformly over the wall thickness, thus reducing the penetration of conductive heat flow and the build-up of thermal stresses close to the hot face. Hence, the wall temperature distribution was much more homogeneous, as observed in Figure 5, avoiding the formation of localized high temperature pockets predicted in the previous CFD analysis, as shown in Figure 4.

Another important aspect is the low concentration of iron oxide and titania in the new refractory composition. These oxides can increase local radiative absorption and participate in flux formation at elevated temperatures, thereby enhancing localized thermal loading in the old refractory. Their substantial reduction in the new refractory helped stabilize the surface emissivity and reduced uneven thermal absorption behaviour along the furnace wall. Consequently, the combustion chamber exhibited a more balanced thermal field with reduced temperature asymmetry and lower probability of thermal runaway near the refractory surface, as shown in Figure 5. Overall, the transition from a silica-dominant refractory to an ultra-high-alumina refractory system fundamentally improved the furnace's resistance to thermo-mechanical failure by enhancing thermal stability, reducing phase-instability-driven cracking, minimizing chemical degradation, and suppressing localized heat accumulation. The absence of hotspot formation in the modified regenerator, therefore, confirms that refractory material composition plays a critical role not only in structural durability but also in controlling the overall thermal behaviour and combustion stability of industrial sulphuric acid regeneration systems.

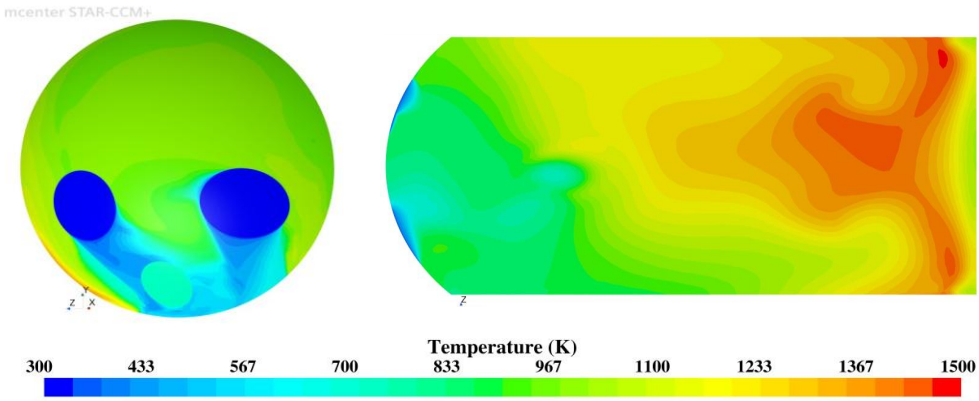

Figure 5. Temperature contour on the curved surface and the midplane of the furnace with modified refractory material

3.1.5 Mass fraction profiles of combustion products

The predicted mass fraction profiles of SO_2 and CO_2 shown in Figures 6 and 7 in the SAR give a detailed insight into the complex thermo-chemical processes taking place in the furnace. The species distributions reflect the efficiency of the sulphuric acid decomposition, droplet evaporation behaviour, turbulent mixing, and gas-phase reaction dynamics inside the regenerator, and combustion performance. Local temperature gradients, residence time, flame structure, and recirculating flow behaviour generated in the combustion chamber have a strong influence on the spatial distribution of these species. The SO_2 mass fraction profile (Figure 6) is dominated by the thermal decomposition pathway of spent sulphuric acid. As the atomised acid droplets enter the high-temperature environment of the furnace, they are rapidly heated by the surrounding combustion gases and intense thermal radiation from the flame zone and refractory surfaces. The moisture is first driven off from the acid, and then the sulphuric acid itself decomposes into SO_3 and H_2O. At the high temperatures within the regenerator, SO_3 further dissociates to SO_2 and oxygen. This results in a significant growth of SO_2 concentration in the primary combustion and decomposition region. The maximum SO_2 mass fractions are usually found in zones with high enough temperature and gas residence time to allow for almost complete decomposition of sulphur-bearing species. This is due to the swirling flow structures generated inside the regenerator that increase the turbulent mixing and keep hot combustion products in the reaction zone for a longer time period. This improves the heat transfer to incoming droplets and enables more efficient acid decomposition. This process of turbulent diffusion and mixing also continues the homogenization of the SO_2 distribution of the combustion products along the flow direction, which implies the stabilization of the chemical conversion process before entering the waste heat recovery section.

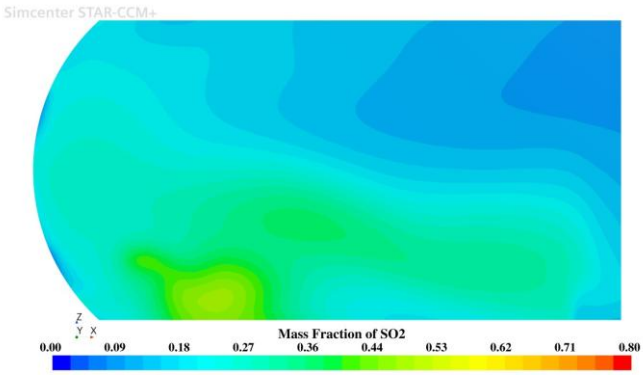

Figure 6. SO_2 mass fraction contour on the central plane of the furnace

The CO_2 mass fraction profile (Figure 7) is essentially set by the oxidation behaviour of hydrocarbon contaminants in the spent acid and the combustion of auxiliary fuel inside the furnace. The high turbulence of the reacting flow in the regenerator causes the combustion intensity to be highest near the burner, where the fuel, oxidiser, and evaporated volatile species mix rapidly. The local temperature increases rapidly here, accelerating oxidation reactions and resulting in high concentrations of CO_2. Therefore, areas with high CO_2 mass fractions correlate very well with regions of high heat release and efficient combustion. The profile also provides an indirect indication of the degree of completeness of combustion in the furnace. The smooth and distributed CO_2 field progressively indicates that the oxidation reactions are proceeding efficiently without significant fuel-rich pockets or incomplete combustion zones. Further downstream the gases, large-scale recirculation together with turbulent transport mechanisms allow for the homogenization of combustion products leading to a more spatially uniform CO_2 distribution over the entire furnace volume.

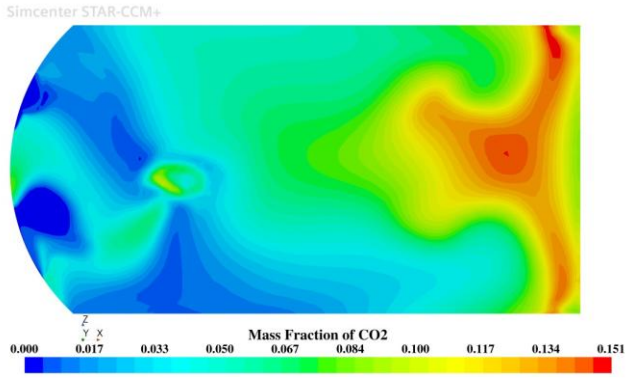

Figure 7. CO_2 mass fraction contour on the central plane of the furnace

One key observation from the species profiles is the tight coupling between the temperature field and the formation of species inside the furnace. High SO_2 and CO_2 concentrations are generally associated with high-temperature regions predicted in the thermal contours, confirming the strong temperature dependence of the combustion intensity and acid decomposition. Similarly, the smooth downstream homogenization of species concentrations demonstrates the effectiveness of turbulent recirculation to stabilize the combustion and improve the residence time. This coupling of combustion chemistry, heat transfer and flow hydrodynamics is of particular relevance in SAR where incomplete decomposition or poor mixing can lead to SO_3 carryover, acid mist formation, localized cooling and unstable furnace operation. Overall, the predicted SO_2 and CO_2 mass fraction distributions confirm that the regenerator is working in a strongly coupled reacting flow environment where combustion, evaporation and decomposition occur continuously and interact with each other. The species profiles confirm the suitability of the combustion chamber design, which ensures good mixing, adequate residence time and thermal stability for effective sulphuric acid regeneration in industrial operating conditions.

4. CONCLUSION

This research evaluates the refractory damage of SAR due to heat accumulation on the curved surface of the furnace using CFD. Advances in CFD algorithms and computing power enabled accurate prediction of thermal hotspots and identification of preventive measures of refractory line failure. A novel CFD methodology is developed for analysing industrial-scale fired furnaces using STAR-CCM+. It employs an Eulerian-Lagrangian multiphase model with liquid fuel evaporation and vapour phase combustion modelled by the Eddy-Breakup approach. The turbulent fluctuations are modelled using the Realizable k-ε turbulence model. The methodology is applied to the SAR plant at IOCL, Paradeep,

Odisha, India, to reduce thermal erosion of refractory brick. The key findings include:

•Initial CFD simulations with base geometries identified thermal hotspots and heat accumulation. The methodology was validated by comparing simulation results with real-time refractory damage locations from IOCL, Paradeep.

•Heat build-up in the curved surface and near the burner zone was identified and addressed by modifying the old refractory bricks with the new aluminium-based refractory bricks.

The modified refractory designs were reviewed with plant engineers, and the upgraded furnaces have since been installed at IOCL, Paradeep. The modified systems are operating without heat accumulation till now, which may significantly extend the lifespan of the refractory lining.

DECLARATION OF INTERESTS

The authors declare that they have no known competing financial interests or personal relationships that could have appeared to influence the work reported in this paper.

ACKNOWLEDGMENT

The authors extend their sincere gratitude to Dr. Meghana Thimmappa, Assistant Professor in the Department of HSS at ITER, SOA University, Bhubaneswar, for her invaluable assistance in refining the manuscript. Her meticulous editing and keen eye for detail significantly improved the English language and corrected any grammatical inconsistencies, ultimately enhancing the quality of the work.

REFERENCES

[1] Guzmán, A.M., Martínez, D.I., González, R. (2014). Corrosion–Erosion wear of refractory bricks in glass furnaces. Engineering Failure Analysis, 46: 188-195. https://doi.org/10.1016/j.engfailanal.2014.09.003

[2] Prestes, E., Medeiros, J., Gomes, D.T., Veiga, J.L.B.C., Pandolfelli, V.C. (2013). Hot-erosion of nano-bonded refractory castables for petrochemical industries. Ceramics International, 39(3): 2611-2617. https://doi.org/10.1016/j.ceramint.2012.09.026

[3] Tang, H., Fang, M., Min, X., et al. (2016). Mechanical properties and solid particle erosion behavior of LaMgAl11O19–Al2O3 ceramic at room and elevated temperatures. Journal of the American Ceramic Society, 99(6): 2138-2146. https://doi.org/10.1111/jace.14205

[4] Wang, X., Fang, M., Zhang, L.C., et al. (2013). Solid particle erosion of alumina ceramics at elevated temperature. Materials Chemistry and Physics, 139(2-3): 765-769. https://doi.org/10.1016/j.matchemphys.2013.02.029

[5] Keshavarz, E., Toghraie, D., Haratian, M. (2017). Modeling industrial scale reaction furnace using computational fluid dynamics: A case study in Ilam gas treating plant. Applied Thermal Engineering, 123: 277-289. https://doi.org/10.1016/j.applthermaleng.2017.05.079

[6] Yang, J.Z., Fang, M.H., Huang, Z.H., et al. (2012). Solid particle impact erosion of alumina-based refractories at elevated temperatures. Journal of the European Ceramic Society, 32(2): 283-289. https://doi.org/10.1016/j.jeurceramsoc.2011.08.017

[7] Agrawal, A., Ghoshdastidar, P.S. (2018). Computer simulation of heat transfer in a rotary lime kiln. Journal of Thermal Science and Engineering Applications, 10(3): 031008. https://doi.org/10.1115/1.4039299

[8] Singh, A.P., Ghoshdastidar, P.S. (2021). Computer simulation of heat transfer in alumina and cement rotary kilns. Journal of Thermal Science and Engineering Applications, 14(3): 031001. https://doi.org/10.1115/1.4051376

[9] Prasad, K., Kadirvell, V.G., Satapathy, L.N., Sanakaranarayana, R. (2017). High temperature erosion of dense refractory castables for CFBC boilers. Interceram - International Ceramic Review, 66(1-2): 24-29. https://doi.org/10.1007/BF03401198

[10] Khamar, L., Hadane, A., Benjelloun, S., Oqaidi, S. (2021). Simulation of sulphur furnace combustion using CFD approach. In Presented at the AMT2020: The 6th International Congress on Thermal Sciences, Khouribga, Morocco, p. 020046. https://doi.org/10.1063/5.0049652

[11] Eskandarzadeh, H., Akbari, G., Yazdi, M.E., Lohrasbi Nichkoohi, A. (2023). Numerical simulation of a high-pressure reactive furnace in recovering sulphur from sour gas. ACS Omega, 8(40): 36744-36752. https://doi.org/10.1021/acsomega.3c03065

[12] Fattahi, M., Ebrahimi, S., Rahimi, M., Gonbadi, M., Hosseini, S.H., Ahmadi, G. (2024). Analyzing burner performance and combustion phenomenon in an olefin plant's industrial furnace: A CFD study. ACS Omega, 9(12): 14500-14519. https://doi.org/10.1021/acsomega.4c00395

[13] Harasek, M., Maier, C., Haberfelner, H. (2010) Investigation of the SO2-production process by combustion of sulphur containing substances using computational fluid dynamics. In Sulphur 2010 Technical Preprints, pp. 219-225.

[14] Mounaam, A., Bichri, A., Oulhiq, R., et al. (2022). Dynamic modeling and simulation of the sulphur combustion furnace in industrial smelter. Processes, 10(12): 2655. https://doi.org/10.3390/pr10122655

[15] Nemalipuri, P., Das, H., Pradhan, M. (2020). Simulation of emission from coal-fired power plant. Advances in Mechanical Engineering: Select Proceedings of ICRIDME 2018, pp. 975-986. https://doi.org/10.1007/978-981-15-0124-1_87

[16] Gopala Krishna, E.D., Shamshoddin, S., Ande, R. (2018). Numerical simulation of fluid flow and heat transfer in a ductile iron ladle during holding and teeming. Journal of Thermal Science and Engineering Applications, 11(1): 011007. https://doi.org/10.1115/1.4041341

[17] Nemalipuri, P., Singh, V., Vitankar, V., Das, H.C., Pradhan, M.K., Jena, S. (2025). Predicting the safety zone and fire dynamics of heptane multiple pool fire in a square dike using flamelet-generated manifold model. Journal of the Brazilian Society of Mechanical Sciences and Engineering, 47(1). https://doi.org/10.1007/s40430-024-05363-2

[18] Nemalipuri, P., Singh, V., Vitankar, V., Das, H.C., Pradhan, M.K. (2024). Numerical prediction of fire dynamics and the safety zone in large-scale multiple pool fire in a dike using flamelet model. Canadian Journal of

Chemical Engineering, 102(1): 11-29. https://doi.org/10.1002/cjce.25094
[19] Nemalipuri, P., Singh, V., Das, H.C., Pradhan, M.K., Vitankar, V. (2023). Consequence analysis of heptane multiple pool fire in a dike. Proceedings of the Institution of Mechanical Engineers, Part C: Journal of Mechanical Engineering Science. https://doi.org/10.1177/09544062231181813
[20] Kumar, A., Nemalipuri, P., Singh, V., et al. (2023). Simulation of natural gas combustor using CFD. Recent Advances in Mechanical Engineering, pp. 667-679. https://doi.org/10.1007/978-981-16-9057-0_72
[21] Nemalipuri, P., Pradhan, D.M.K. (2018). Prediction of air pollutants emitting from chimney of a CHP using CFD. International Journal of Scientific and Engineering Research, 9(4): 105-110.
[22] Mirzaei, M., Clausen, S., Wu, H., et al. (2023). Investigation of erosion in an industrial cyclone preheater by CFD simulations. Powder Technology, 421: 118424. https://doi.org/10.1016/j.powtec.2023.118424
[23] Melo, P.H.R.V.D., Peixoto, J.J.M., Galante, G.S., et al. (2019). The influence of flow asymmetry on refractory erosion in the vacuum chamber of a RH degasser. Journal of Materials Research and Technology, 8(5): 3764-3771. https://doi.org/10.1016/j.jmrt.2019.06.036
[24] Abumounshar, N.M., Ibrahim, S., Raj, A. (2021). A detailed reaction mechanism for elemental sulphur combustion in the furnace of sulphuric acid plants. Canadian Journal of Chemical Engineering, 99(11): 2441-2451. https://doi.org/10.1002/cjce.24185
[25] Bhagat, P.K. (2015). Department of Mechanical Engineering National Institute of Technology Rourkela Odisha-769008, India May 2015. Mechanical Engineering.
[26] Zhao, L., Wang, T. (2009). Investigation of potential benefits of using bricks of high thermal capacity and conductivity in a rotating calcining kiln. Journal of Thermal Science and Engineering Applications, 1(1): 011009. https://doi.org/10.1115/1.3192772
[27] Zhou, C.Q., Huang, D.F., Zhao, Y., Chaubal, P. (2010). Computational fluid dynamics analysis of 3D hot metal flow characteristics in a blast furnace hearth. Journal of Thermal Science and Engineering Applications, 2(1): 011006. https://doi.org/10.1115/1.4002195